Mon. Not. R. Astron. Soc. **000**, 000–000 (0000) Printed 27 June 2008 (MN LATEX style file v2.2)

Angular momentum−Large-scale structure alignments in ΛCDM models and the SDSS

Dante J. Paz[1], Federico Stasyszyn[1,2], Nelson D. Padilla [3]
[1] *Instituto de Astronomía Teórica y Experimental IATE (UNC-CONICET), Observatorio Astronómico Córdoba, Francisco N. Laprida 922, Córdoba, Argentina.*
[2] *Max-Planck-Institut fuer Astrophysik MPA, Karl-Schwarzschild-Str. 1, Garching, Germany.*
[3] *Departamento de Astronomía y Astrofísica, Pontificia Universidad Católica de Chile, Vicuña Mackenna 4860, Santiago 22, Chile.*

Accepted 25 June 2008. Received 24 June 2008; in original form 25 April 2008

ABSTRACT

We study the alignments between the angular momentum of individual objects and the large-scale structure in cosmological numerical simulations and real data from the Sloan Digital Sky Survey, Data Release 6. To this end we measure anisotropies in the two point cross-correlation function around simulated halos and observed galaxies, studying separately the 1- and 2-halo regimes. The alignment of the angular momentum of dark-matter haloes in ΛCDM simulations is found to be dependent on scale and halo mass. At large distances (2-halo regime), the spins of high mass haloes are preferentially oriented in the direction perpendicular to the distribution of matter; lower mass systems show a weaker trend that may even reverse to show an angular momentum in the plane of the matter distribution. In the 1-halo term regime, the angular momentum is aligned in the direction perpendicular to the matter distribution; the effect is stronger than for the 1-halo term and increases for higher mass systems.

On the observational side, we focus our study on galaxies in the Sloan Digital Sky Survey, Data Release 6 (SDSS-DR6) with elongated apparent shapes, and study alignments with respect to the major semi-axis. We study five samples of edge-on galaxies, the full SDSS-DR6 edge-on sample, bright galaxies, faint galaxies, red galaxies, and blue galaxies (the latter two consisting mainly of ellipticals and spirals respectively). Using the 2-halo term of the projected correlation function, we find an excess of structure in the direction of the major semi-axis for all samples; the red sample shows the highest alignment ($2.7 \pm 0.8\%$) and indicates that the angular momentum of flattened spheroidals tends to be perpendicular to the large-scale structure. These results are in qualitative agreement with the numerical simulation results indicating that the angular momentum of galaxies could be built up as in the Tidal Torque scenario. The 1-halo term only shows a significant alignment for blue spirals ($1.0 \pm 0.4\%$), consistent with the 1-halo results from the simulation but with a lower amplitude. This could indicate that even though the structure traced by galaxies is adequate to study large-scale structure alignments, this would not be the case for the inner structure of low mass haloes, $M \leqslant 10^{13} h^{-1} M_{\odot}$, an effect apparently more important around red $g - r > 0.7$ galaxies.

Key words: Cosmology: Galaxies – Angular Momentum – Large Scale Structure of the Universe

1 INTRODUCTION

In the current paradigm of large-scale structure formation in the Universe it is well established that the angular momentum of dark-matter (DM) halos is determined early in the history of the Universe by the gravitational interaction between the quadrupole of the collapsing proto-halo region and the surrounding matter. This was first formulated for the hierarchical theory of structure formation by White (1984), Doroshkevich (1970), and Peebles (1969), and it is claimed that this is a natural consequence of the perturbative treatment of the gravitational instability scenario (Porciani, Dekel & Hoffman (2002a)). Several inher-

ent properties to the tidal torque process (Tidal Torque Theory, TTT) have been noticed and studied in the literature. For instance it is expected from TTT, and also supported to some degree by N-body simulations, that the angular momentum starts growing linearly with time (Catelan & Theuns 1996b; Peebles 1969; White 1984), and that later on this process looses efficiency after the halo turnaround. This is due to the reduction of halo inertia by collapse, and to the continued expansion of the neighboring matter responsible for the tidal torque.

There are several analytic studies of the TTT scenario (White 1984; Doroshkevich 1970; Peebles 1969; Catelan & Porciani 2001), as well as semi-analytic approaches (Catelan & Theuns 1996a), and fully non-linear work using cosmological simulations (Barnes & Efstathiou 1987; Sugerman, Summers & Kamionkowski 2000; Porciani, Dekel & Hoffman 2002a,b; Peirani, Mohayaee, & de Freitas Pacheco 2004; Nagashima & Gouda 1998). The agreement is that the resulting halo population is poorly rotationally supported; the velocity dispersion at virialisation is found to be the most important mechanism for halo equilibrium. As a result, the distribution of spin parameters[1] is log-normal which peaks at quite low values, $\lambda_{med} \simeq 0.035$ (Bullock et al. 2001; Gardner 2001; D'Onghia & Burkert 2004; Maccio' et al. 2006; Bett et al. 2007). Unfortunately it is not possible to obtain a direct measurement of spin parameters in actual galaxies. Despite this, Hernandez et al. (2007) used indirect methods to derive distributions of galaxy spin parameters consistent with theoretical predictions.

From an observational point of view, it can be easier in some cases to determine the direction of the angular momentum of a given galaxy rather than its amplitude. There has been a recent increase in the interest concerning the possibility of galaxy alignments with the large scale structure. Such studies are important to test the already well developed TTT, and to asses the possibility that such correlations affect the results of cosmic shear measurements. Regarding the former, TTT produces noisy predictions due to the non-linear nature of the accretion processes of clumpy matter (Vitvitska et al. 2002; Porciani, Dekel & Hoffman 2002a), on scales below the coherent scale of flows predicted by linear theory. The second tests for the effects on cosmic shear studies used to analyse weak lensing, may answer whether there is an intrinsic alignment in the structure traced by galaxies that could result in a spurious contribution to the shear power spectrum (Hirata et al. 2007; Bridle & Abdalla 2007; Takada & White 2004; King & Schneider 2003; King 2005; Heymans & Heavens 2003; Heymans et al. 2004; Brown et al. 2002; Catelan, Kamionkowski & Blandford 2001; Crittenden et al. 2001; Croft & Metzler 2000; Jing 2002). Several authors have searched for galaxy alignments in the super-galactic plane (de Vaucouleurs 1953), extending out to several tens of megaparsecs from our Galaxy, and more recently on large galaxy surveys (Hirata et al. 2007, 2004; Lee & Erdogdu 2007; Lee & Pen 2007; Mandelbaum et al. 2006). Lee & Erdogdu (2007) claim a direct evidence of an alignment between galaxy position angle in 2MRs and the tidal field deduced from galaxy positions.

An interesting approach to the analysis of galaxy alignments is to use the radial direction to the centres of voids as characteristic directions in the large scale structure. It is well known that as they evolve, large voids tend to be rounder, a behaviour which is opposite to that shown by bound structure. Negative density perturbations in the initial fluctuation field that will later become voids, are characterised by a decreasing asphericity as the expansion of the Universe proceeds, as is shown by Sheth & van de Weygaert (2004) (and references therein). Taking advantage of this particular characteristic of voids, it is possible to study the whether galaxy or halo angular momenta are aligned with the void shells just by considering the angle with respect to the direction to the void centre. This is the approach used by Trujillo, Carretero & Patiri (2006) applied to the SDSS and 2dFGRS galaxy redshift surveys, and by Brunino et al. (2007), Cuesta et al. (2008) and Patiri et al. (2006) to numerical simulations. Trujillo, Carretero & Patiri (2006) find with a high level of confidence that spiral galaxies located on the shells of the largest cosmic voids have rotation axes that lie preferentially on the void surface, in agreement with the simulation results of Brunino et al. (2007); Cuesta et al. (2008); Patiri et al. (2006). Other more general methods that also take into account alignments with large scale filaments in numerical simulations show similar results (Aragón-Calvo et al. 2007; Hahn et al. 2007a,b).

In this paper we present results from a study of alignments between individual objects and their surrounding structure in quantitative concordance with TTT predictions and previous observational results. We use a novel approach to study alignments with the large-scale structure using as a reference the galaxy/dark matter halo angular momentum. Using numerical simulations we study alignments predictions in a Cold Dark Matter model with a cosmological constant (ΛCDM), and compare such predictions with the results obtained from the Sloan Digital Sky Survey, Data Release 6 (SDSS-DR6, Adelman-McCarthy et al., 2007). To this end we use the galaxy two point correlation function applied both, in its three-dimensional definition to the full numerical simulation and in its projected version to mimic the observational limitations. The latter allows us to determine that we should be able to detect the expected low signal alignments, even in small galaxy samples. This allows us to measure the alignment of galaxies and halos over wide ranges in mass and separation, and also to quantify the dependence of this alignment on halo mass, galaxy colour and luminosity.

This paper is organised as follows. Section 2 presents the numerical simulation and the statistical tools we will use in this work; it also presents an analysis of the impact of the observational biases on the detection of alignments. Section 3 contains the analysis of observational samples of galaxies from the Sloan Digital Sky Survey. The comparison between models and observations as well as the discussion of the results is presented in Section 4, and Section 5 contains the final conclusions from this work.

[1] The dimensionless spin parameter as defined by Peebles (1969) is $\lambda = L\sqrt{|E|}/GM^{5/2}$, where E is the total internal energy of the halo and L and M are its angular momentum and mass respectively. This number can be understood as a measure of the importance of rotational velocity vs. velocity dispersion as the dominant support mechanism of a halo

2 ANISOTROPIES IN THE 3D CORRELATION FUNCTION

In this section we analyse the three-dimensional two-point correlation function, using cluster-particle pairs, measured using ΛCDM numerical simulations, taking into account the orientation with respect to the centre halo angular momentum. To this end, we have run two periodic simulations of 500 and 60 h^{-1}Mpc computational box sizes, for a flat low-density Universe, with a matter density $\Omega_{\rm m} = 1 - \Omega_\Lambda = 0.3$, Hubble constant $H_\circ = 70$ km s^{-1} Mpc^{-1}, and normalisation parameter $\sigma_8 = 0.8$. The particle resolutions are $m_{\rm p} \geqslant 7.2 \times 10^{10}\, h^{-1}\, M_\odot$ for the large simulation, and $m_{\rm p} \geqslant 1.2 \times 10^8\, h^{-1}\, M_\odot$ for the small one. The identification of particle clumps has been carried out by means of a standard friends-of-friends algorithm with a percolation length given by $l = 0.17\ \bar{\nu}^{-1/3}$, where $\bar{\nu}$ is the mean number density of DM particles. Both simulations have been performed using the first version of the GADGET code developed by Springel et al. (2001). We consider halos with at least 30 and 100 particles in the large and small simulations, respectively, in order to ensure an accurate measurement of the halo angular momentum.

The spatial halo-particle cross-correlation function $\xi(r)$ which we will use in this section, measures the excess probability with respect to a random distribution, that a DM particle will reside at a distance r away from a given halo centre, in the volume element dV,

$$dP = \bar{\nu}\,[1 + \xi(r)]\,dV. \qquad (1)$$

A standard method to measure $\xi(r)$ in a simulation box is to count pairs at a given distance bin, and then normalise this number by the expected number of pairs for a constant number density of objects. In our measurements we perform these counts stacking pairs depending on the angle between their position relative to the centre halo and its angular momentum. We consider tree cases, (i) using all pairs regardless of this angle (spherical shell volumes, isotropic case), (ii) using all pairs subtending an angle from the angular momentum less than a given threshold θ_1 (parallel case), and (iii) adding pairs at lower inclinations than a limit angle θ_2 from the perpendicular plane to the angular momentum (perpendicular case). We choose the threshold angles, for the parallel and perpendicular cases mentioned above (θ_1 and θ_2, respectively), so that the volumes in each case are the same. This can be achieved by setting, $\sin(\theta_2) = 1 - \cos(\theta_1) = \chi$, and choosing a value for the threshold parameter χ. Selecting $\chi \leqslant 0.5$ implies angles $\theta_1 \leqslant 60^o$ and $\theta_2 \leqslant 30^o$. Throughout this paper we use $\chi = 0.5$.

Errors in the correlation function are estimated using the jacknife technique, with a total of 50 subsamples for the numerical simulation (20 jacknifes for the SDSS data analysis). We find that our errors are stable for this number of jacknife subsamples (we tested from 20 to 100) and does not produce underestimations. In the case of quotients between correlation functions, we apply the jacknife technique to the actual measurement of the ratio. We adopt the jacknife technique since it has been reported to provide similar error estimates to those obtained from independent samples (see for instance, Padilla et al., 2004).

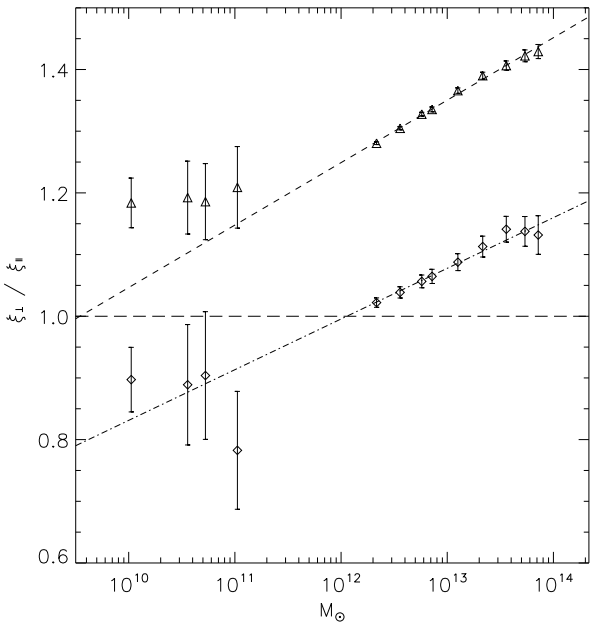

Figure 2. Ratios between correlation functions for neighbors in the directions perpendicular and parallel to the halo angular momentum. Diamonds (triangles) correspond to the ratio over the 2-halo (1-halo) term scales.

2.1 Simulation results

The analysis of alignments of structure with the angular momentum of DM haloes presents a first difficulty in that in order to obtain a reliable and stable direction for the halo spin, it is often necessary to use a large number of particles per halo. We find that using 30 particles provides reasonable results, but this imposes a rather high lower limit to halo masses of $2.2 \times 10^{12}\, h^{-1}\, M_\odot$ for the large simulation, and $3.6 \times 10^9\, h^{-1}\, M_\odot$ for the smaller one. We analised the distribution of angular momentum parameters and find that the reported high λ tail (Bett et al., 2007) due to low number of particles per halo, is not present in any of our samples of DM haloes. We notice that the clustering signal in the small simulation on large scales may be affected by the small box size.

From this point on, we will centre most of our analysis on samples of DM haloes with different masses. From the small simulation we draw four DM halo subsamples separating haloes of different mass starting at a minimum of 100 particles or $M \geqslant 1.2 \times 10^{10}\, h^{-1}\, M_\odot$ (the lowest mass sample considered includes haloes of up to 300 particles each; we do not use haloes of lower masses even though we are still above the minimum number of particles we consider safe to consider). Nine samples are drawn from the large simulation and contain DM haloes with more than 30 particles. The subsample with the most massive haloes starts at 1000 particle members corresponding to $M \geqslant 7.2 \times 10^{13}\, h^{-1}\, M_\odot$.

The left panels of Figure 1 show the cross-correlation function between low mass DM haloes and DM particles (top-left) in the directions parallel and perpendicular to their angular momenta, and in all directions (diamonds,

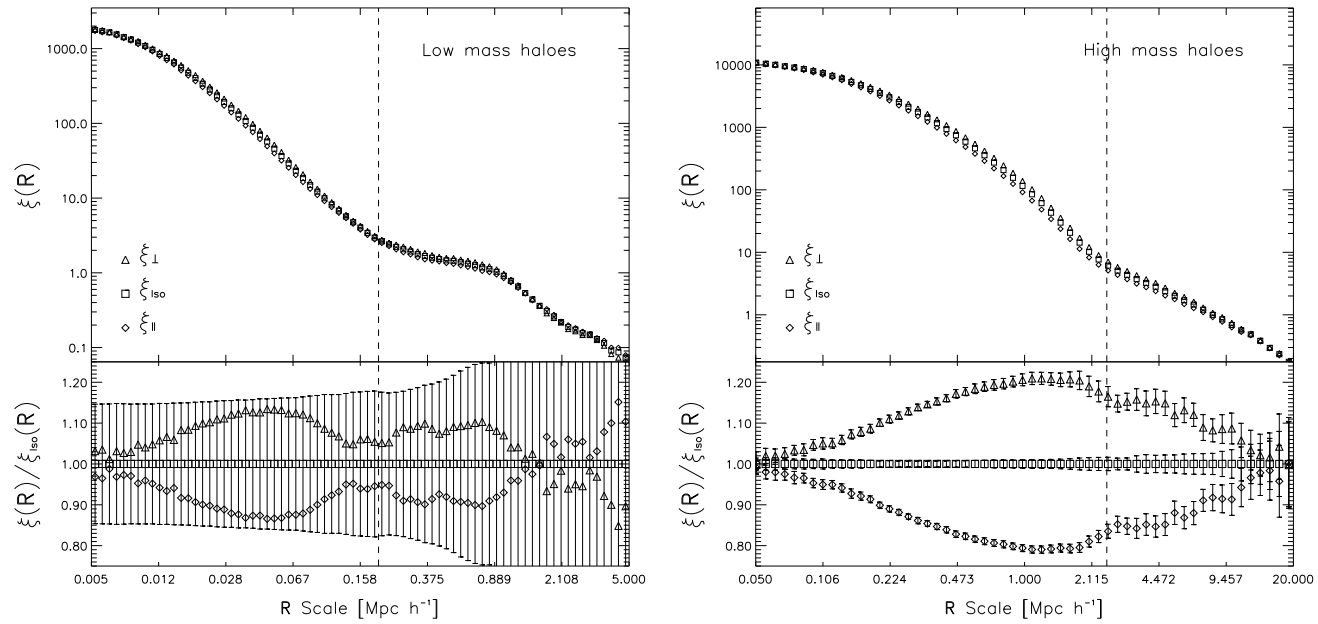

Figure 1. Left panel: Spatial Halo−Dark-matter correlation function of low mass haloes in the small numerical simulation. The triangles correspond to the correlation function between haloes and neighbors in the direction perpendicular to the angular momentum of the centre haloes. The diamonds show the results when using tracers along the direction of the angular momentum, and the squares the results when all neighbors are taken into account. The lower left panel shows the ratio between the correlation functions shown in the top-left panel and the results using all neighbors. Right panel: same as left panel, for a high mass DM halo subsample from the large simulation.

triangles and squares, respectively). The lower panel shows the ratios between these three estimates and the correlation function considering all neighbors; their relative amplitudes help identify alignments in either direction. As can be seen, the relative amplitudes of the correlation function when using neighbors in the directions parallel and perpendicular to the angular momentum of the DM halo are different; for small separations $R < 1\mathrm{h}^{-1}\mathrm{Mpc}$, there is an excess of correlation in the direction perpendicular to the angular momentum of up to a 20% effect (between correlations parallel and perpendicular to the angular momentum, lower panel), whereas for larger separations the alignment diminishes and shows a tendency to reverse (although, as can be seen in the figure, errors are larger at these separations); we come back to this later in this section where we use a higher signal estimator for alignments.

When using higher mass DM haloes, the effect is also present with an even higher difference and statistical significance between the structure in the direction of the angular momentum and perpendicular to it (Right panels of Figure 1). In this case, neighbors in the direction perpendicular to the angular momentum show more correlation, and there is a clear tendency for this alignment to decrease with separation, which goes from almost a 50% effect on relative amplitudes (lower panel) at small separations to about $< 5\%$ at large separations. Note that the alignment does not change at large separations as seemed to be the case for low mass haloes, even at $R = 20\mathrm{h}^{-1}\mathrm{Mpc}$ compared to $R = 5\mathrm{h}^{-1}\mathrm{Mpc}$ analised in the low mass halo sample.

Notice that the halo-particle cross-correlation functions in Figure 1 show the characteristic 1- and 2-halo terms reported in several previous measurements of both observational (e.g. Zehavi et al., 2004, Cooray, 2005) and numerical simulations (Zheng et al., 2004); these two regimes are separated in the figure by the vertical dashed lines. This separation is obtained by measuring the scale at which the correlation function is seen to shift between these two regimes (there is a local minimum in the first derivative of the correlation function). It can be seen that the alignment signal shows a clear transition from the 1- to the 2-halo regime; in particular, low mass haloes show indications of a different angular momentum−large-scale alignment behaviour in the 2-halo regime, suggesting an important relationship between alignment and halo term. This can be interpreted as different physical mechanisms producing the alignment in the 1- and 2-halo terms.

We make quantitative estimates of the alignments for the 1- and 2-halo terms separately from the cross-correlation functions shown in Figure 1 as well as from the other samples of DM haloes with intermediate masses (for a total of 13 samples of varying halo masses). We only consider pairs that are separated by a distance at least as large as the transition between regimes for the 2-halo term, and at shorter separations for the 1-halo calculations.

In order to avoid effects of covariance between the correlation function bins to some extent, we make global 1- and 2-halo term estimates of the ratios between the correlation functions in the directions perpendicular and parallel to the angular momentum of haloes, using all the halo-particle pairs separated by distances within the 1- and 2-halo ranges (i.e. we do not use the narrow bins in $\log_{10}(r)$ used to calculate the cross-correlation functions). We acknowledge that

traces of covariance will still be present between the 1- and 2-halo term ratios. We present these results in Figure 2, where triangles show the 1-halo term ratio between correlation functions for neighbors in the directions perpendicular and parallel to the halo angular momentum; Diamonds correspond to the 2-halo term. The horizontal long dashed line at $\xi_{\parallel}/\xi_{\perp} = 1$ corresponds to the isotropic case. The datapoints at masses lower than $10^{12}h^{-1}M_{\odot}$ correspond to the small numerical simulation, and show larger errors due to both, the smaller simulated volume, and the lower amplitude of clustering characterising low mass haloes.

As can be seen, the 1-halo term always shows more structure in the direction perpendicular to the angular momentum, and more so for larger masses, whereas the 2-halo term shows a similar behaviour with the possible exception of low mass haloes, whose angular momenta tend to point in the direction of the large-scale structure (although with a low statistical significance). The alignments are detected at about a $5-\sigma$ level for the higher mass halo subsamples drawn from the large simulation. As in the 2-halo regime, low mass haloes show considerably higher errors.

In the case of low mass halos ($M \simeq 10^{10}h^{-1}M_{\odot}$) in the 2-halo term regime (diamonds in Figure 2), the alignment signal is the opposite to that of higher mass haloes (a $10 \pm 5\%$ effect). This anti-alignment signal fits in well with the overall tendency for this quotient $\xi_{\parallel}/\xi_{\perp}$ to increase with mass, which can be fit by a log-linear relation which crosses the unit value at $M \simeq 10^{12}h^{-1}M_{\odot}$. This mass limit suggest a change in the alignment signal in qualitative agreement (regarding the alignment direction) with results on simulations by Hahn et al. (2007a), with masses above and below the typical mass scale for collapse $M_{*} = 5.5 \times 10^{12.5}h^{-1}M_{\odot}$ at $z = 0$. The best-fit log-linear relation for the 2-halo term results is shown in Figure 2 (dash dotted line), and corresponds to,

$$\xi_{\parallel}/\xi_{\perp} = (0.95 \pm 0.01) + (0.082 \pm 0.008) * [log_{10}(M) - 11.5] \quad (2)$$

For the 1-halo term, the dependence of alignment on mass is well adjusted by (dashed line on Figure 2),

$$\xi_{\parallel}/\xi_{\perp} = (0.95 \pm 0.01) + (0.082 \pm 0.008) * [log_{10}(M) - 11.5] \quad (3)$$

The 2-halo term effect can be understood within the framework of TTT, specially for the high mass haloes, which readily show that their angular momentum is perpendicular to the present-day mass distribution. It seems that for high enough mass haloes, the local large-scale structure still describes the original tidal field. In the case of low mass haloes, the alignment seems to reverse. This result can be understood by an intuitive non-linear effect beyond the abilities of TTT, for example if these haloes have formed recently in filaments, from the merger of material arriving from voids surrounding these elongated structures.

The 1-halo term results indicate that regardless of halo mass, the structure within dark-matter haloes is preferentially aligned with the plane perpendicular to the angular momentum, with a higher statistical significance and signal than the 2-halo term.

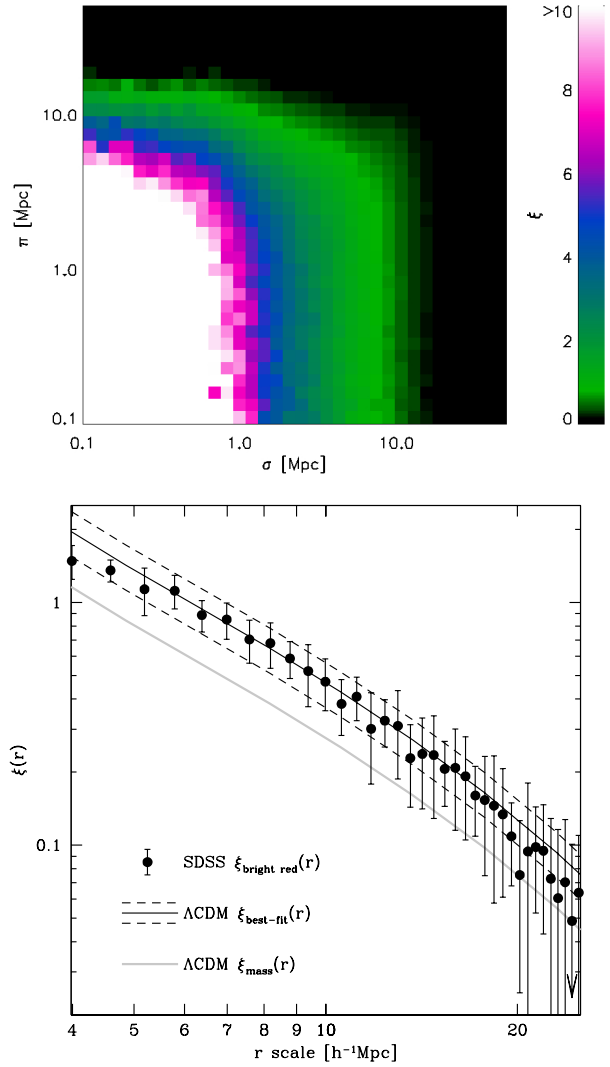

Figure 4. Top panel: Correlation function around "edge-on" red spiral galaxies in the SDSS-DR6 (sample O3), in the directions parallel and perpendicular to the line of sight. The colour indicates the amplitude of the correlation function (see the figure key). Bottom panel: real-space correlation function for the same sample of galaxies, obtained as explained in the text (symbols with errorbars), and the best-fit ΛCDM real-space correlation function (black lines). The dashed lines show the range of correlation function amplitudes allowed by the errors in the data. The gray thick line shows the mass real-space correlation function in the ΛCDM model.

2.2 Simulating observational biases in the numerical simulation

It can be difficult to estimate the angular momentum of real galaxies. In the case of the SDSS-DR6, which we use in this work, the only information that can allow us to obtain an estimate of the direction of the angular momentum is the photometry of galaxy images, specially for spiral galaxies but also for ellipticals. We assume that spiral discs or flattened spheroids are perpendicular to the angular momentum of galaxies and therefore, edge-on galaxies (either disks or spheroidals) will be more likely to have their angular mo-

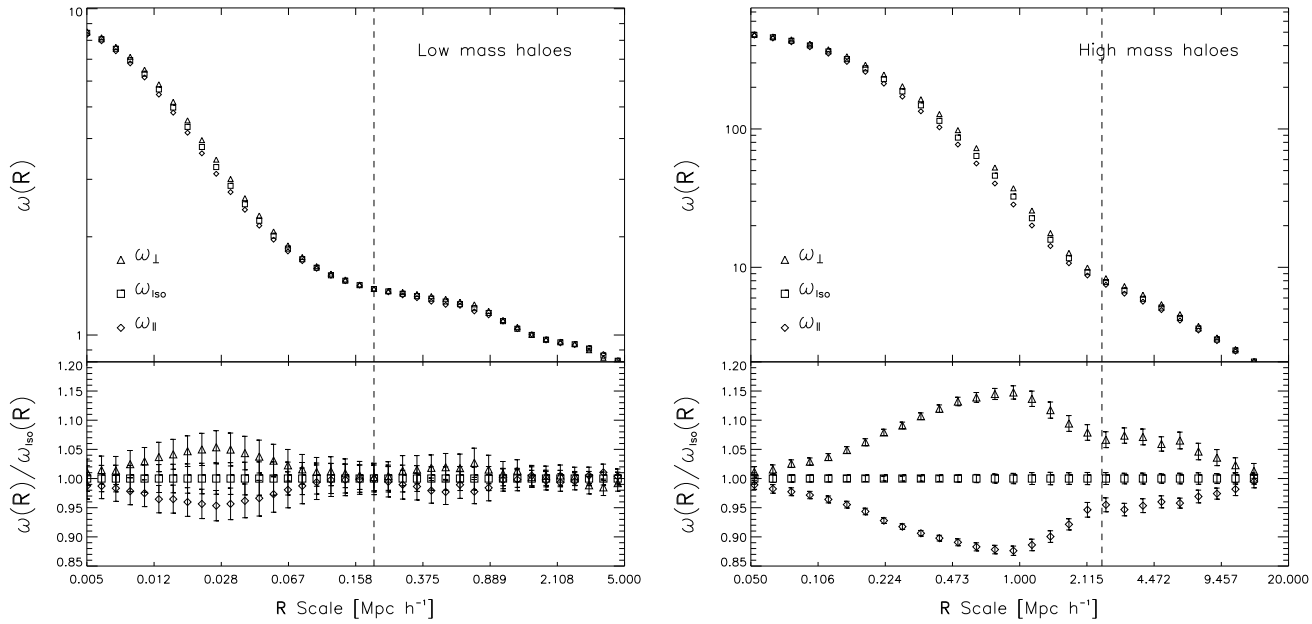

Figure 3. Left panels: projected correlation functions around "edge-on" low mass haloes in the small numerical simulation (top-left), in the directions perpendicular and parallel to the angular momentum of centre haloes (triangles and diamonds symbols, respectively). Ratios between these projected correlation functions are shown in the bottom-left panel. Right panels: same as left panels for high mass haloes in the large numerical simulation.

mentum on the plane of the sky. Then, one can calculate the cross-correlation function for neighbors in the projected direction parallel and perpendicular to the direction of the angular momentum of the centre galaxies, in redshift slices around them, assuming all these neighbors to be at the same distance than the centre galaxy. This slice needs to be defined so that it avoids projecting large amounts of foreground and background structures while still allowing enough numbers of neighbors to obtain good statistics.

In order to assess whether the alignments found in the previous subsection are identifiable in observational catalogues analised this way, we reproduce the procedure mentioned in the previous paragraph in our analysis of the numerical simulation which consists on projecting the structure onto the plane of the sky, assuming all objects within $\Delta v = 750$km/s from the centre haloes to be exactly at the same distance from the observer.

Therefore we only use information from two cartesian coordinates in the simulation, x and y, and transform the third, z, into a velocity component by multiplying z by the Hubble Constant and adding the z component of the peculiar velocity. In order to complete the emulation of redshift space effects suffered by observational surveys, we apply this transformation to the simulation particles as well as to the halo catalogue. We then select "edge-on" haloes from the simulation, by requiring that their angular momentum is at an angle less than 60^o from the sky, represented by the $x-y$ plane [2]. We can then study two projected correlation functions centred in these objects using DM particles, (i) a correlation function calculated using pairs that subtend an angle with the projected angular momentum of less than 30^o, which we call the parallel projected correlation function ($\omega_{||}$), and (ii) a perpendicular projected correlation function ($\omega_{\perp}$) obtained by counting pairs that subtend an angle greater than 60^o from the projected angular momentum.

Figure 3 shows the results from this procedure. The left panels show the results for low mass haloes in the small simulation (projected correlation functions in the top-left, and ratios in the bottom-left), whereas the right panels show the results for high mass haloes in the large simulation. As can be seen, these results are qualitatively consistent with the alignment signal found in the previous subsection using the full three-dimensional correlation function, which indicates that projected correlation functions are a suitable tool to detect this effect. The overall effect has a lower amplitude; high mass haloes show a ratio between structure in the directions perpendicular and parallel to their angular momenta of about a 30% excess (for the 3D case, this was above 50%) and low mass haloes show a 10% effect (compared to $20-30\%$), which makes this detection a slightly more difficult task.

3 OBSERVATIONS

Galaxies with spiral and flattened spheroidal shapes projected onto the sky give a handle on their orientation with respect to the line of sight and, therefore, it is possible to estimate in a statistical sense the direction of their angular momentum. Spiral galaxies with round projected shapes are likely discs seen face-on and therefore their angular momenta point in the direction perpendicular to the plane of the sky;

[2] Such angle threshold is equivalent to a ratio of 0.5 of the ellipsoidal image semi-axes for a perfect thin disc.

Table 1. Observational samples from the SDSS-DR6 spectroscopic main galaxy sample. The first and second column indicate the sample name and number of galaxies in them, the third column indicates the number density, and the fourth column the host-halo mass.

Sample	Members	$n/10^{-3}\mathrm{h}^{-3}\mathrm{Mpc}^3$	$\mathrm{Log}_{10}(M_{\rm host}/\mathrm{h}^{-1}M_\odot)$
O1	132000	10.4 ± 0.8	$12.50^{+0.30}_{-0.54}$
O2	59300	6.50 ± 0.12	$13.06^{+0.19}_{-0.27}$
O3	72700	5.50 ± 0.12	$11.40^{+0.56}_{-0.80}$
O4	10900	7.15 ± 0.17	$12.19^{+0.45}_{-1.17}$
O5	1400	1.10 ± 0.20	$12.67^{+0.28}_{-0.48}$

elongated projected shapes indicate discs seen edge-on, and therefore their angular momenta point in the direction perpendicular to the long axis of the ellipsoid. On the other hand, elliptical galaxies with round projected shapes can either be nearly intrinsically spherical or flattened spheroids seen face-on; however, elongated ellipticals are more likely flattened spheroids seen edge-on since recent results on intrinsic elliptical shapes indicate that these are more commonly oblate rather than prolate spheroids (e.g. Padilla & Strauss, 2008). Therefore, elongated ellipticals are likely to be also characterised by angular momenta pointing in the direction of the plane of the sky roughly perpendicular to the major axis of the ellipsoid, as is the case for edge-on spiral galaxies. These last two types of galaxies will be the centre of the following analysis. We notice that the amplitude of the angular momentum of flattened spheroidals is likely to have a low amplitude relative to that of spiral galaxies.

The sample we selected to carry out our analysis is the spectroscopic SDSS-DR6, which contains a total of $\simeq 580,000$ galaxies with spectroscopic redshifts and photometry in five bands, u, g, r, i, z, as well as parameters determining the projected galaxy shapes consisting of the two semi-axes and the position angle of the ellipse that once convolved with the PSF (seeing) provides the best match to the photometric image of each individual galaxy. In the remainder of this paper, we only consider SDSS-DR6 galaxies within the redshift range $0.02 < z < 0.09$.

We study the alignment signal in the observational data for different subsamples defined by galaxy colour and luminosity in order to detect trends that can be associated to the results from the numerical simulation. The subsamples we study are sample O1, consisting of all the edge-on galaxies with axial ratio $b/a < 0.7$ in the SDSS-DR6; O2, red galaxies with $g - r > 0.7$; O3, blue galaxies with $g - r < 0.7$; O4, faint galaxies with $M_r > -19.5$; and O5 composed by bright galaxies with $M_r < -19.5$. The selection of subsamples is done so as to ensure a number of target galaxies to allow good statistics (> 1000); the number of galaxies in each sample is shown in Table 1, where we also show the galaxy number density calculated out to the redshift of completeness of each sample.

In order to characterise in a quantitative way the subsamples selected from the SDSS-DR6, we calculate the median mass of ΛCDM haloes predicted to show the same 2-halo regime clustering amplitude as the galaxies in each subsample. We follow the procedure used in several previous works (cf. Croft et al. 1999, Padilla et al., 2001) consisting on calculating the auto-correlation function of galaxies in two coordinates, one parallel (σ) and one perpendicular (π) to the line of sight, $\xi(\sigma, \pi)$, and integrating over the π direction to avoid the effect of redshift space distortions. The result from this integration is the projected correlation function (see for instance, Croft et al., 2001), $\Xi(\sigma)$,

$$\Xi(\sigma) = 2 \int_{\pi_{min}}^{\pi_{max}} \xi(\sigma, \pi) d\pi, \quad (4)$$

which in turn can be inverted to obtain the real-space correlation function via

$$\xi(r) = \frac{-1}{\pi} \sum_{j \geqslant i} \frac{\Xi(\sigma_{j+1}) - \Xi(\sigma_j)}{\sigma_{j+1} - \sigma_j} \ln \left(\frac{\sigma_{j+1} + \sqrt{\sigma_{j+1}^2 - \sigma_i^2}}{\sigma_j + \sqrt{\sigma_j^2 - \sigma_i^2}} \right), \quad (5)$$

where the sum is performed over the bins in σ where the projected correlation function has been calculated. The masses of host haloes can then be obtained by finding the bias between the resulting real-space correlation functions and the matter correlation functions in a ΛCDM cosmology (both in the 2-halo regime), which we obtain by Fourier transforming the non-linear matter power spectrum (from Peacock & Smith, 2000) for the same cosmological parameters used in the numerical simulations. With an estimate of the bias, the mass of the host haloes can be found by using the Sheth, Mo & Tormen (2001) formalism. Note that this procedure is equivalent to measure the real-space halo-halo correlation function for haloes of different masses (Sheth, Mo & Tormen, 2001, Padilla & Baugh, 2002), with the advantage of avoiding large uncertainties from small samples of haloes restricted to narrow ranges of halo mass in the simulation. We show one example of this procedure in Figure 4, where we find the mass of haloes with an equivalent clustering amplitude to the sample of red galaxies in the SDSS-DR6 (O2). In this figure, the top panel shows the auto-correlation function, $\xi(\sigma, \pi)$, of O2 galaxies, and the lower panel the resulting real-space correlation function (symbols) and the best fit ΛCDM curve. From this analysis we find that red galaxies in the SDSS-DR6 (with $b/a < 0.7$) are consistent with haloes of a median mass of $\log_{10}(M/h^{-1}M_\odot) = 13.06^{+0.19}_{-0.27}$. This provides us with a quantitative way to compare the SDSS-DR6 subsamples to the halo samples in the numerical simulations. Also, in order to infer this scale for our observational samples, we will use the dependence of the 1- to 2-halo term transition on DM halo mass measured in our the numerical simulations.

The other SDSS-DR6 galaxy samples are fitted by the correlation function of DM haloes of masses indicated in Table 1. Notice that our study covers over one and a half decades in the host-halo mass of SDSS-DR6 galaxies.

As we demonstrated in the previous section both, the large scale structure and alignments surrounding galaxies, can be studied using the projected correlation function, $\omega(\sigma)$, measured in terms of the projected separation, σ. We now apply this method to our samples of edge-on galaxies, and compare the outcome from using tracers in the direction parallel and perpendicular to the inferred angular momentum, to detect differences between the structure along these two directions.

The projected correlation functions are calculated using galaxies in a given subsample, cross-correlated to the full spectroscopic SDSS-DR6 catalogue. As in the 2-dimensional analysis carried out in the numerical simulations, we calculate the cross-correlation for edge-on galaxies selected so

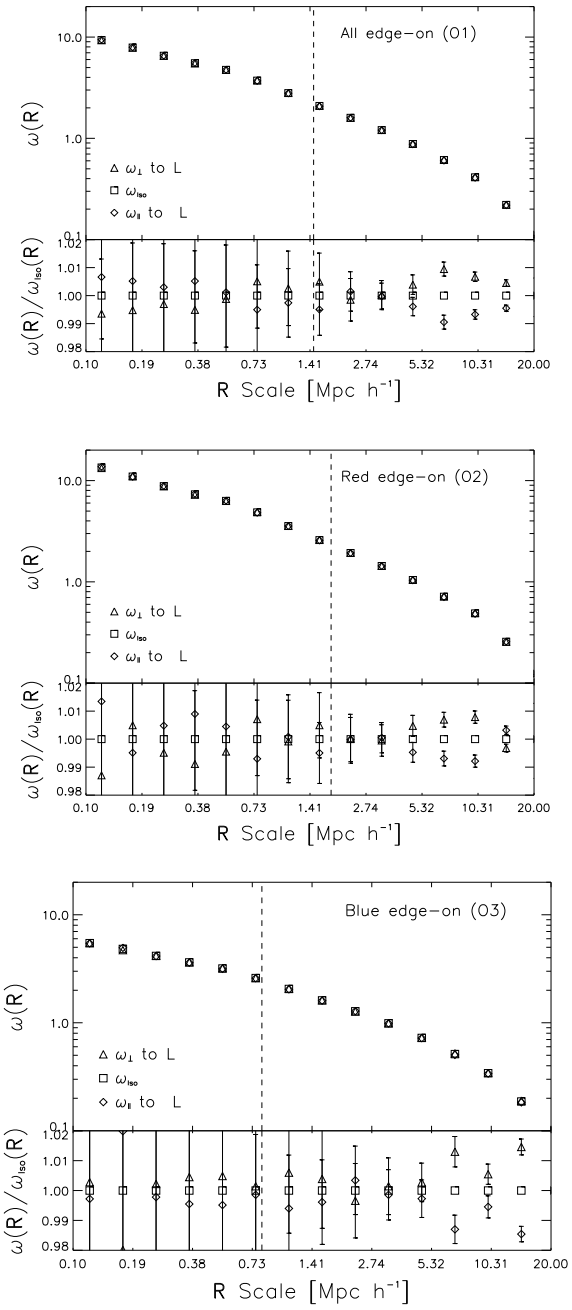

Figure 5. Correlation functions around "edge-on" galaxies in the SDSS-DR6, in the direction perpendicular and parallel to the angular momentum of centre haloes (triangles and diamonds, respectively). Top panel corresponds to sample O1 (full SDSS-DR6), middle panel to O2 (red galaxies), and bottom panel to sample O3 (blue galaxies). The vertical dashed lines show the transition from the 1- to the 2-halo regimes corresponding to the host-halo mass obtained from the real-space correlation function of the different samples.

that $b/a < 0.7$. Note that in the numerical simulation we used an angle between the halo angular momentum and the line of sight of 60^o, which in the case of a perfect thin disk is equivalent to $b/a = 0.5$, but is larger for a thick disk as is the case of the intrinsic shapes of spiral galaxies or flattened ellipsoids (Padilla & Strauss, 2008).

Figure 5 shows the measured correlation functions for Edge-on galaxies for the three subsamples that show significantly different signatures of alignments with the angular momentum. These are the full sample of edge-on spirals, O1 (top panel), the red galaxy sample, O2 (middle panel), and the blue galaxies, sample O3 (bottom panel). As in the results for the numerical simulation, triangles show the correlation with galaxies in the direction of the angular momentum, diamonds in the perpendicular direction, and squares, when using all neighbors. A first glance at the shapes of these correlation functions indicates that there is not as clear a transition between the 1- and 2-halo terms as in the results from the numerical simulations (see Fig. 3); in these samples the main effect is a transition to a roughly constant slope for the $\log(\xi)$ vs. $\log\sigma$ relation. This may be an indication that the internal structure of haloes is not traced in the same way by galaxies in the SDSS-DR6 and DM particles in the ΛCDM model. Regarding the alignments, it can be seen that the three subsamples show the large-scale structure preferentially aligned with the direction perpendicular to the angular momentum, specially for the 2-halo regime, as was found in the cosmological simulation. The difference between the two correlation functions is roughly a $2-\sigma$ detection over the range of scales defined by $2 < r/\mathrm{h}^{-1}\mathrm{Mpc} < 20$ and corresponds to about a $2-4\%$ effect.

The analysis of the faint and bright samples (O4 and O5, respectively) provide alignment results in quantitative agreement with the full galaxy sample, O1, with results within a $1-\sigma$ difference. Therefore, we will not show results from these two samples in the remainder of this work.

A more quantitative comparison between observational and simulation results is presented in the following section.

4 DISCUSSION

In order to compare quantitatively the alignments found in the observations and in the numerical simulation, we use the transition scale from the 1- to the 2-halo regimes inferred in the previous section to determine the degree of alignment found in these two regimes separately. As in section 2.1, we estimate ratios between the correlation functions in the directions perpendicular and parallel to the estimated galaxy angular momentum direction, using all pairs within the 1- and 2-halo regimes. This can then be directly compared to the results from the numerical simulations for projected correlations.

Figure 6 shows the ratios between projected correlation functions in the directions parallel and perpendicular to the angular momentum as a function of halo mass. The results from the numerical simulations are shown as diamonds, and the results from the observational samples at the corresponding host-halo masses are shown as filled symbols. We show results for samples O1 (full SDSS-DR6, filled squares), O2 (red galaxies, filled upward pointing triangles), and O3 (blue galaxies, filled downward pointing triangles). The top panel shows the results from the analysis of the 1-halo term, the lower panel from the 2-halo term. For the 2-halo term regime the resulting alignment signals for observational samples are $1.8 \pm 0.5\%$ for the full sample O1, $2.7\pm0.7\%$ for the red galaxy sample 02, and $0.8\pm0.4\%$ for the blue galaxy sample 03. The 1-halo term regime shows align-

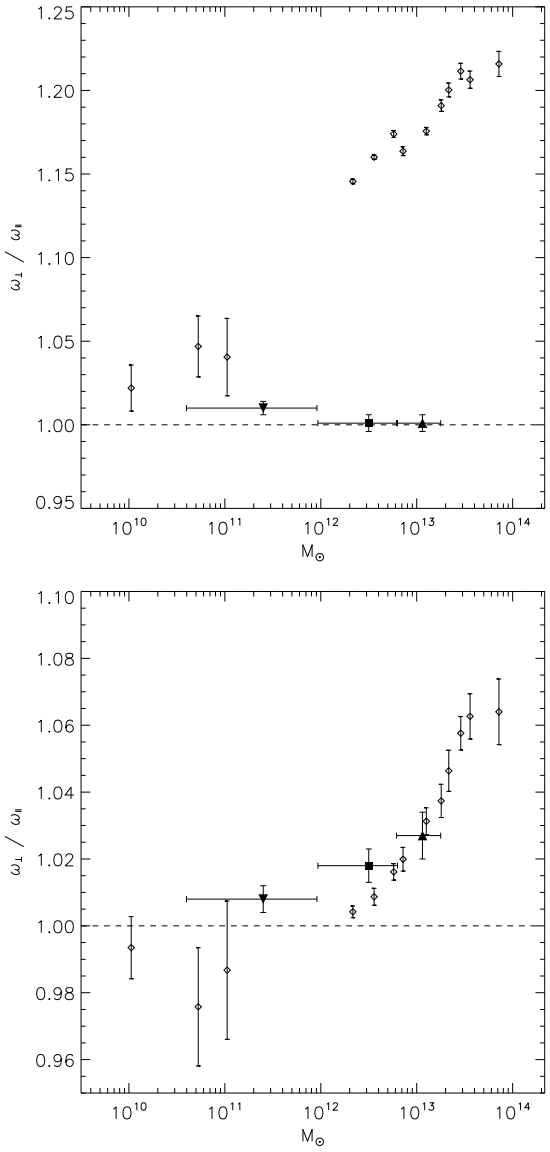

Figure 6. Ratios between projected correlation functions in the directions parallel and perpendicular to the projected angular momentum as a function of halo mass in the numerical simulation (open diamonds). Galaxy samples O1 (all galaxies), O2 (red galaxies), and 03 (blue galaxies), are shown as filled symbols: squares, upward pointing triangles, and downward pointing triangles, respectively. Top panel: ratios for the 1-halo term. Bottom panel: ratios for the 2-halo term.

ments of $0.1 \pm 0.5\%$, $0.1 \pm 0.5\%$, and $1.0 \pm 0.4\%$ for samples O1, O2, and O3, respectively. As can be seen, the alignment found in the 2-halo term is consistent between observational samples and the numerical simulation (differences are at a maximum a $1-\sigma$ effect).

This agreement indicates that TTT in combination with hierarchical clustering are a viable theory since not only the angular momentum of galaxies points in the direction perpendicular to the surrounding large-scale structure, but also the amplitude of the effect is similar to what is found in the numerical simulations. It should be noticed that this would also indicate that the direction of the angular momentum in galaxies in these samples is tracing the angular momentum of the host halo. The results for the 1-halo term, on the other hand, show that galaxies follow a different behaviour than DM haloes as was suspected from the lack of a clear transition to the 1-halo term in the shape of the SDSS projected correlation functions; at the range of masses corresponding to the observational samples, the simulated haloes show very significant alignments, whereas the only sample of galaxies that a shows non-zero alignment is that composed by blue galaxies (although still lower than the simulation data, at a regime of low expected alignments). The combination of the 1- and 2-halo term results could indicate that the general galaxy population in the SDSS-DR6 which our samples are cross-correlated to, can be used as good tracers of the large-scale structure (i.e. have not suffered important changes to deviate from the angular momentum of their host haloes) but would fail to serve as indicators of the internal distribution of matter in their host DM haloes; different astrophysical processes could produce this effect, specially for such low $M \simeq 10^{13} h^{-1} M_\odot$ halo masses[3]. This result is particularly interesting since blue galaxies do show traces of an alignment in the same direction as the numerical simulation, which has a number of possible explanations. For instance, the angular momentum of red galaxies could be subject to a reshuffle that adds enough noise to loose its alignment with the internal halo structure while leaving the large-scale signal almost intact, an effect could also involve a positional reshuffle within the halo structure; another possibility is that red galaxies are able to rearrange their companion galaxies inside DM haloes. However, a more quantitative analysis is required in order to find the true underlying cause for this behaviour. We acknowledge the possibility that observational biases not included in our analysis of the numerical simulation are still affecting these measurements.

5 CONCLUSIONS

We study the alignments between the angular momentum of individual objects and the large-scale structure in cosmological numerical simulations and in the SDSS-DR6. The angular momentum of DM haloes in ΛCDM simulations is found to be preferentially oriented in the direction perpendicular to the distribution of matter in the range of separations corresponding to the 1- and 2-halo terms. These results are in agreement with the Tidal Torque Theory.

We find that more massive haloes show a higher degree of alignment, and that the 1-halo term shows a much higher alignment than the 2-halo term. We find a maximum 1-halo alignment of $\sim 40\%$ for haloes of $\simeq 10^{14} h^{-1} M_\odot$; at low masses, the 1-halo signal seems to tend to a constant value of 20%. The 2-halo term alignment shows a maximum signal of $\simeq 15\%$ at high masses, and possible inversion at low masses where the angular momentum might even preferentially point in the direction of the distribution of mass on large scales. The latter would be consistent with low mass

[3] There is observational evidence that groups of galaxies with masses above this limit are characterised by intrinsic shapes consistent to those found in numerical simulations (Paz et al. 2006); however it is difficult to directly measure the shapes of lower mass systems due to discreteness effects.

groups formed not too long ago from mass distributed in the surrounding areas of the already-formed filaments or walls.

The alignment of the angular momentum with the large-scale structure found for low mass systems is in agreement with previous works by (Trujillo, Carretero & Patiri 2006) on redshift surveys, and by Brunino et al. (2007); Patiri et al. (2006); Cuesta et al. (2008); Aragón-Calvo et al. (2007); Hahn et al. (2007a,b) on simulations. The main difference with these previous studies relies in that we quantify the strength of the alignment in terms of the two-point correlation function, as a function of halo mass. In particular, we find that a log-linear relation fits the dependence of alignment on mass, for both, the 1- and 2-halo term regimes. For the latter we observe a turning point between an angular momentum pointing in the direction perpendicular to the structure, to no-alignment, and then to a regime where the angular momentum is contained by the plane defined by the surrounding structure. This occurs at a mass $\simeq M_*$, in qualitative agreement with previous studies (Bailin & Steinmetz 2005; Hahn et al. 2007a,b).

Combining our results for the 1- and 2-halo terms for haloes in the numerical simulation, namely that the angular momentum of haloes is perpendicular to the bulk of the matter within haloes (1-halo term), and also to the surrounding large-scale structure (for masses $> M^*$), our findings are in agreement with previous works who find that the major axis of haloes is usually aligned with the large-scale structure (Gottlöber & Turchaninov 2006, Bett et al. 2007, Faltenbacher et al. 2002; Kasun & Evrard 2005; Bailin & Steinmetz 2005; Colberg, Krughoff & Connolly 2005; Altay, Coldberg & Croft 2006; Basilakos et al. 2006; Ragone-Figueroa & Plionis 2007, and references therein). Regarding the 1-halo term signal, our results are also in qualitative agreement with recent results by Knebe et al. (2008) on the alignments of substructure within dark matter halos.

We use numerical simulations to reproduce the procedure that can be applied to observational samples using projected correlation functions. We find that the alignment signal diminishes considerably but that it can still be measured.

Therefore, we study edge-on galaxies in the SDSS-DR6, and assign the direction perpendicular to the major semi-axis as the direction of the angular momentum. Since our samples are restricted to objects with flattened apparent shapes ($b/a < 0.7$), these include both edge-on spiral galaxies and flattened spheroids. We are able to detect alignments in all our galaxy samples. These include the full SDSS-DR6 edge-on galaxies, a sample composed by blue ($g - r < 0.7$) galaxies, the sample of red ($g - r > 0.7$) galaxies, and a sample of faint and another composed by bright galaxies. The latter two samples show a quantitative agreement with the results from the full sample of edge-on galaxies in the SDSS.

In all cases we find a significant excess of structure in the direction perpendicular to the angular momentum for the 2-halo term, in good agreement with the numerical simulation results. The 1-halo term results show either a null or lower alignment signal than expected from the analysis of projected correlations in the numerical simulation. This would suggest the effects of astrophysical processes acting so that galaxies do not follow the DM structure inside low mass haloes of $\leqslant 10^{13} h^{-1} M_\odot$ or lower masses, a result that complements previous studies of high mass groups in the SDSS with $M \gtrsim 10^{13} h^{-1} M_\odot$, where galaxies are found to follow the internal DM structure (e.g. Paz et al., 2006). This effect is apparently more important for red, $g-r > 0.7$ galaxies, indicating that there may be interesting astrophysical effects at work at low mass dark-matter haloes which could produce changes in the orientation of galaxy angular momenta, or the spatial re-distribution of galaxies within them.

ACKNOWLEDGMENTS

DJP acknowledges receipt of a fellowship of Consejo Nacional de Investigaciones Cientifico Tecnicas and the support of the European Union's ALFA-II programme, through LENAC, the Latin American European Network for Astrophysics and Cosmology. FAS acknowledges the receipt of an International Max-Planck Research School on Astrophysics fellowship. NDP was supported by a Proyecto FONDECYT Regular 1071006. This work was supported in part by Fondap "Center for Astrophysics" at Universidad Católica de Chile. The authors are very grateful to Manuel Merchán and Cintia Ragone, who kindly provided the numerical simulations and the "Friends of Friends" Code, respectively, used in this work. We acknowledge helpful discussions with Diego Garcia Lambas, Manuel Merchán and Ariel Sanchez. We are also grateful to the anonymous Referee, and to Manolis Plionis, Bernardo Cervantes Sodi, Oliver Hahn and Sebastien Peirani, whose feedback helped us improve this work in a significant way. This research has made use of the NASA Astrophysics Data System.

REFERENCES

Adelman-McCarthy, J., et al. 2007, in press (arXiv:0707.3413).
Altay G., Colberg J. M., Croft R. A. C., 2006, MNRAS, 370, 1422
Aragón-Calvo M. A., van de Weygaert R., Jones B. J. T., van der Hulst J. M., 2007, ApJ, 655, L5
Aryal B., Saurer W., 2005, A&A, 425, 431
Bailin J., Steinmetz M., 2005, ApJ, 627, 647
Barnes J. & Efstathiou G., 1987, ApJ, 319, 575
Basilakos S., Plionis M., Yepes G., Gottlöber S., Turchaninov V., 2006, MNRAS, 365, 539
Bett P., Eke V., Frenk C. S., Jenkins A., Helly J., Navarro J. 2007,MNRAS,376,215
Bridle S., Abdalla F. B., 2007, ApJ, 655, 1
Brown M. L., Taylor A. N., Hambly N. C., Dye S., 2002 MNRAS, 333, 501
Brunino R., Trujillo I., Pearce F.R., Thomas P.A., 2007, MNRAS, 375, 184
Bullock J. S., Dekel A., Kolatt T. S., Kravtsov A. V., Klypin A. A., Porciani C., Primack J. R. 2001, ApJ, 555, 240
Catelan P., Kamionkowski M., Blandford R. D., 2001, MNRAS, 320, 7
Catelan P., Porciani C., 2001, MNRAS, 323, 713
Catelan P., Theuns T., 1996a, MNRAS, 282, 436
Catelan P., Theuns T., 1996b, MNRAS, 282, 455
Colberg J. M., Krughoff K. S., Connolly A. J., 2005, MNRAS, 359, 272

Crittenden R. G., Natarajan P., Pen U., Theuns T., 2001, ApJ, 559, 552
Croft R., Dalton G., Efstathiou G. 1999, MNRAS, 305, 547.
Croft R. A. C., Metzler C. A., 2000, ApJ, 545, 561
Cuesta A. J., Betancort-Rijo J. E., Gottlöber S., Patiri S. G., Yepes G., Prada F., 2008, MNRAS, 385, 867
D'Onghia E., Burkert A., 2004,ApJ, 612, 13
Doroshkevich A. G., 1970, Astrofisika, 6, 581
Eisenstein D.J. & Loeb A., 1995, ApJ, 439, 520
Faltenbacher A., Gottlöber S., Kerscher M., Müller V., 2002, A&A, 395, 1
Flin P., Godlowski W., 1989, SvAL, 15, 374
Gardner J. P., 2001,ApJ, 557, 616
Garrido J. L., Battaner E., Sanchez-Saavedra M. L.,Florido E., 1993, A&A, 271, 84
Gottlöber S., Turchaninov V., 2006, EAS, 20, 25
Hahn O., Porciani C., Carollo C. M., Dekel A., 2007, MNRAS, 375, 489
Hahn O., Carollo C. M., Porciani C., Dekel A., 2007, MNRAS, 381, 41
Han C., Gould A., Sackett P. D., 1995, ApJ, 445, 46
Heavens A. & Peacock J., 1988, MNRAS, 232, 339
Hernandez X., Park C., Cervantes-Sodi B., Choi Y.-Y., 2007, MNRAS, 375, 163
Heymans C., Heavens A., 2003, MNRAS, 339, 711
Heymans C., Brown M., Heavens A., Meisenheimer K., Taylor A., Wolf C., 2004, MNRAS, 347, 895
Hirata C. M., Mandelbaum R., Seljak U., Guzik J., Padmanabhan N., Blake C., Brinkmann J., Budvari T., Connolly A., Csabai I., Scranton R., Szalay A. S., 2004, MNRAS, 353, 529
Hirata C. M., Mandelbaum R., Ishak M., Seljak U., Nichol R., Pimbblet K. A., Ross N. P., Wake D.,2007, MNRAS, 381, 1197
Hoffman Y., 1986,ApJ, 301, 65
Hoffman Y., 1988,ApJ, 329, 8
Hu F. X., Yuan Q. R., Su H. J., Wu G. X., Liu Y. Z., 1998, ApJ, 495, 179
Hu F. X., Wu G. X., Song G. X., Yuan Q. R., Okamura S., 2006, Ap&SS, 302, 43
Jing Y. P., 2002, MNRAS, 335, 89
Kasun S. F., Evrard A. E., 2005, ApJ, 629, 781
King L.,2005, A&A, 441, 47
King L., Schneider P., 2003, A&A, 398, 23
Knebe A., Yahagi H., Kase H., Lewis G., Gibson B. K., 2008, arXiv, 805, arXiv:0805.1823, MNRAS Letter, in press
Lee J., Erdogdu P., 2007,ApJ, 671,1248
Lee J., Pen U., 2007, ApJ, 670,1
Maccio' A., Dutton A., van den Bosch F., Moore B., Potter D., Stadel J., 2006, MNRAS, 378, 55
Mackey J., White M., Kamionkowski M., 2002, MNRAS, 332, 788
Mandelbaum R., Hirata C. M., Ishak M., Seljak U., Brinkmann J., 2006, MNRAS, 367, 611
Nagashima M., Gouda N., 1998, MNRAS, 301, 849
Navarro J. F., Abadi M. G., Steinmetz M., 2004, ApJ, 613, 41
Padilla N., & Baugh C.M. 2002, MNRAS, 329,431.
Padilla N., & Strauss M. 2008, MNRAS, submitted, arXiv:0802.0877.
Padilla N., Merchan M., Valotto C., Lambas D.G., Maia M. 2001, ApJ, 554, 873.
Padilla N., et al. (The 2dFGRS Team) 2004, MNRAS, 352, 211
Patiri S. G., Cuesta A. J., Prada F., Betancort-Rijo J., Klypin A., 2006, ApJ, 652, L75
Paz D., Lambas D.G., Padilla N., Merchan M. 2006, MNRAS, 366, 1503.
Peacock J., & Smith R. 2000, MNRAS, 318, 1144.
Peebles P. J. E., 1969, ApJ, 155, 393
Peirani S., Mohayaee R., de Freitas Pacheco J. A., 2004, MNRAS, 348, 921
Porciani C., Dekel A., Hoffman Y., 2002a, MNRAS, 322, 325
Porciani C., Dekel A., Hoffman Y., 2002b, MNRAS, 332,339
Quinn T. & Binney J., 1992, MNRAS, 255, 729
Ragone-Figueroa C., Plionis M., 2007, MNRAS, 377, 1785
Ryden B.S., 1988,ApJ, 329, 589
Sheth R. K., van de Weygaert R., 2004, MNRAS, 350, 517
Sheth R., Mo H.J., & Tormen G. 2001, MNRAS, 323, 1.
Sugai H., Iye M., 1995, MNRAS, 276, 327
Sugerman B., Summers F. J., Kamionkowski M., 2000, MNRAS, 311,762
Takada M., White M., 2004, ApJ, 601, 1
Trujillo I., Carretero C., Patiri S.G., 2006,
Vitvitska M., Klypin A. A.,Kravtsov A. V., Wechsler R. H., Primack J. R., Bullock J. S.,2002,ApJ,581,799
White S. M. D., 1984, ApJ,286, 38
de Vaucouleurs G., 1953, AJ, 58, 30